A Model For Sedimentation In Inhomogeneous Media. I. Dynamic Density Gradients From Sedimenting Co-Solutes

Peter Schuck

Division of Bioengineering & Physical Science, ORS, OD, National Institutes of Health, Bethesda, Maryland 20892.

[#]Address for Correspondence:

Dr. Peter Schuck
National Institutes of Health
Bldg. 13, Rm. 3N17
13 South Drive
Bethesda, MD 20892-5766,USA
Phone: 301 435-1950
Fax: 301 480-1242
Email: pschuck@helix.nih.gov

Abstract

Macromolecular sedimentation in inhomogeneous media is of great practical importance. Dynamic density gradients have a long tradition in analytical ultracentrifugation, and are frequently used in preparative ultracentrifugation. In this paper, a new theoretical model for sedimentation in inhomogeneous media is presented, based on finite element solutions of the Lamm equation with spatial and temporal variation of the local density and viscosity. It is applied to macromolecular sedimentation in the presence of a dynamic density gradient formed by the sedimentation of a co-solute at high concentration. It is implemented in the software SEDFIT for the analysis of experimental macromolecular concentration distributions. The model agrees well with the measured sedimentation profiles of a protein in a dynamic cesium chloride gradient, and may provide a measure for the effects of hydration or preferential solvation parameters. General features of protein sedimentation in dynamic density gradients are described.

<u>Introduction</u>

The sedimentation of macromolecules through inhomogeneous media is a process frequently

encountered in the practice of centrifugation. Density gradient techniques in preparative

ultracentrifuges have a great importance as general biochemical tools. In analytical

ultracentrifugation, density gradient sedimentation has a long history for the study of nucleic acids

[1-3], the molar mass and buoyant density of proteins [4], and it is still applied in a variety of

studies with topics ranging from the composition of genomes [5-7] to the characterization of

protein-detergent and protein-lipid complexes [8, 9]. Smaller self-forming density gradients

generated by the centrifugal field are the basis of analytical zone centrifugation [10, 11], and

gradients in solvent density and viscosity may also be generated inadvertently at high centrifugal

fields when using high concentrations of a sedimenting co-solute, such as sucrose. In the field of

synthetic polymer chemistry, isopycnic density gradient ultracentrifugation is an important assay

for the characterization of macromolecules and particles, for example in industrial processes [12].

The theoretical prediction and the analysis of macromolecular transport in density

gradients is significantly more complex than the standard sedimentation in homogeneous solvents

for thermodynamic and computational reasons. A variety of models were proposed in earlier

studies. Several authors addressed the migration of a sedimenting band in a hypothetical pre-

existing density and/or viscosity gradient [13-16]. As part of their pioneering theoretical work on

the characterization and analysis of macromolecular sedimentation profiles in the ultracentrifuge,

Dishon, Weiss and Yphantis have first considered the evolution of the solvent density distribution

with time [17]. They used an empirical formula for the relaxation kinetics of the distribution of a

co-solute acting as densifier, and solved the macromolecular redistribution in the dynamic gradient

with the flow equation for macromolecular sedimentation and diffusion in the centrifugal field, the

Lamm equation [18]. In this work, the simplifying assumption of a rectangular geometry was made [17]. Sartory et al. have used a finite-difference solution of the Lamm equation to describe the sedimentation of the small co-solute, and developed approximate analytical expressions for the sedimentation and diffusion of a thin band of macromolecules in the dynamic density gradient, using an equilibrium pertubation technique [19]. Minton has developed a detailed finite-difference method for predicting the non-ideal sedimentation of CsCl, and described a finite-difference algorithm for the simulation of a macromolecular species in the density gradient [20].

In the last decade, the analysis of transport processes in analytical ultracentrifugation underwent significant development. The application of improved mathematical and computational tools now permits the efficient and precise solution of the Lamm equation, which can be used to characterize macromolecular sedimentation coefficients, molar masses, size-distributions and molecular interactions [21-32]. However, this development was constrained to the sedimentation in homogeneous solvents.

In the present paper, a general model is proposed for macromolecular sedimentation in inhomogeneous media. It is based on finite-element solutions of the Lamm equation with a dynamic description of the local density and viscosity, derived from the non-ideal sedimentation of a co-solute. It can also be applied to the sedimentation in compressible solvents, which is described in the second paper of this series [33]. The model is implemented in the software SEDFIT and can be used for the prediction of macromolecular sedimentation, as well as for analysis of experimentally measured macromolecular concentration profiles from the analytical ultracentrifuge. The model is tested with experimental data from the sedimentation of a protein in CsCl solution, and several features of macromolecular sedimentation in inhomogeneous media are described.

Theory

Finite element solution of the Lamm equation in inhomogeneous solvents

The Lamm equation describes the sedimentation and diffusion of a macrosolute in the sector-shaped volume of the analytical ultracentrifuge:

$$\frac{\partial c}{\partial t} = \frac{1}{r}\frac{\partial}{\partial r}\left[rD\frac{\partial c}{\partial r} - s\mathbf{w}^2 r^2 c \right] \tag{1}$$

with c (r,t) denoting the concentration at a distance r from the center of rotation and at time t, ω the angular velocity, D the diffusion coefficient, and s the sedimentation coefficient. Although it is strictly not valid for three-component systems [34], it may be used as a first approximation for macromolecular sedimentation for cases where interactions between the macrosolute and co-solute can be neglected or approximated as a constant apparent change in the partial-specific volume of the macrosolute. In this approximation, gradients in density and viscosity due to the redistribution of co-solute will be treated as a background on which macromolecular sedimentation and diffusion according to Eq. 1 takes place. Limitations of this approximation will be discussed below.

If we consider the effect of locally varying solvent viscosity η and density ρ on the macromolecular sedimentation, it is useful to relate the local macromolecular transport parameters to those under standard conditions:

$$D_{\exp}(r,t) = \frac{\eta_{20,w}}{\eta(r,t)} D_{20,w} =: \alpha(r,t)D_{20,w} \tag{2a}$$

$$s_{\exp}(r,t) = \frac{\mathbf{h}_{20,w}}{\mathbf{h}(r,t)}\left(\frac{1 - \mathbf{f}'\,\mathbf{r}(r,t)}{1 - \bar{v}\,\mathbf{r}_{20,w}} \right)s_{20,w} =: \mathbf{a}(r,t)\mathbf{b}(\,r,\,t)\,s_{20,w} \tag{2b}$$

with the partial-specific volume of the macromolecule $\bar{v}$, with the standard conditions denoted with the index 20,w (for water at 20 °C), with the apparent partial-specific volume ϕ' (which includes hydration and preferential solvation), and with the abbreviation α denoting the inverse of

the relative viscosity, and with β denoting the relative buoyancy. It should be noted that if the density of the macromolecule $1/\bar{v}$ is close to the solvent density, changes in the relative buoyancy can be very large even at small changes in density. The thermodynamically correct form of the buoyancy factor is the density increment $(d\rho/dc)_\mu$ [35]. It is expressed here in an equivalent form of a buoyancy factor with an apparent partial-specific volume $(1 - \boldsymbol{f}' \boldsymbol{r}(r,t))$, from which preferential interaction coefficients with of water and co-solute may be calculated [36] (see discussion).

Although the Lamm equation (Eq. 1) does not have an analytical solution, it can be solved very efficiently by finite element techniques [24, 25, 37]. Following the method outlined in [24], we can approximate the concentration distribution c(r,t) as a superposition of elements P_k

$$c(r,t) \approx \sum_{k=1}^{N} c_k(t) P_k(r,t) \tag{3}$$

which are based on a grid of N radial points that divide the sample from meniscus m to bottom b:

$$P_1(r,t) = \begin{cases} (r_2 - r)/(r_2 - r_1) & for \quad r_1 \leq r \leq r_2 \\ 0 & else \end{cases} \tag{4a}$$

$$P_N(r,t) = \begin{cases} (r - r_{N-1})/(r_N - r_{N-1}) & for \quad r_{N-1} < r \leq r_N \\ 0 & else \end{cases} \tag{4b}$$

and for k = 2,...,N:

$$P_k(r,t) = \begin{cases} (r - r_{k-1})/(r_k - r_{k-1}) & for \quad r_{k-1} < r \leq r_k \\ (r_{k+1} - r)/(r_{k+1} - r_k) & for \quad r_k < r \leq r_{k+1} \\ 0 & else \end{cases} \tag{4c}$$

As introduced first by Claverie [37], the elements P_k can be constant and equidistant triangular hat functions ($r_{k+1} = r_k + \Delta r$). A more efficient and numerically more stable choice of elements, in particular for small D, is a moving frame of reference, in which the radial grid points r are

logarithmically spaced and time-dependent [24]. If the $r_k(t)$ evolve exponentially according to $r_k(r) = r_{k,0}\exp(s_G\omega^2(t-t_0))$ (with s_G denoting a sedimentation coefficient), they mimic the sedimentation of a non-diffusing particle and can provide a frame of reference that is translated and stretched so that the sedimentation term in Eq. 1 disappears and Eq. 1 reduces to the description of diffusion alone. Details on efficient spatial and temporal discretization schemes can be found in [24]. The following discussion will proceed in a general way with non-equidistant and time-dependent elements P_k, in which the equations for a Claverie grid are contained as a special case with $\partial P_k/\partial t = 0$.

Analogous to the macromolecular concentration, we can also use the elements P_k to express the local viscosity term α and the relative buoyancy β as

$$\alpha(r,t) = \sum_{k=1}^{N} \alpha_k(t)P_k(r,t)$$
$$\beta(r,t) = \sum_{k=1}^{N} \beta_k(t)P_k(r,t)$$

(5)

Multiplication of both sides of Eq. 1 with an element P_k and volume integration from meniscus to bottom (using integration by parts and taking advantage of the vanishing total flux at meniscus and bottom) leads to

$$\int_m^b \frac{\partial c}{\partial t} P_k r dr = s_{20,w}\mathbf{w}^2 \int_m^b \mathbf{abc}\frac{\partial P_k}{\partial r} r^2 dr - D_{20,w}\int_m^b \mathbf{a}\frac{\partial c}{\partial r}\frac{\partial P_k}{\partial r} r dr$$

(6)

Inserting Eqs. 3 and 5 leads to the set of linear equations

$$\sum_j \frac{dc_j}{dt}\int_m^b P_j P_k r dr + \sum_j c_j \int_m^b \frac{\partial P_j}{\partial t} P_k r dr =$$

$$s_{20,w}\mathbf{w}^2 \sum_j c_j \sum_{l,n} a_l \mathbf{b}_n \int_m^b P_l P_n P_j \frac{\partial P_k}{\partial r} r^2 dr - D_{20,w}\sum_j c_j \sum_l a_l \int_m^b P_l \frac{\partial P_j}{\partial r}\frac{\partial P_k}{\partial r} r dr$$

(7)

which can be written in matrix form

$$\sum_j \left(\frac{dc_j}{dt} \mathbf{B}_{kj} + c_j s_G \mathbf{A}_{kj}^{(3)} \right) = \sum_j c_j \left(s_{20,w} \omega^2 \sum_{l,n} a_l \beta_n \mathbf{A}_{ln,kj}^{(2*)} - D_{20,w} \sum_l a_l \mathbf{A}_{l,kj}^{(1*)} \right) \qquad (8)$$

In Eq. 8, the matrices $\mathbf{B}_{kj}$ and $s_G \mathbf{A}_{kj}^{(3)}$ are as described in [24], and analytical expressions for the

new matrices $\mathbf{A}^{(1*)}(t) = \sum_l \alpha_l \mathbf{A}_{l,kj}^{(1*)}$ and $\mathbf{A}^{(2*)}(t) = \sum_{l,n} \alpha_l \beta_n \mathbf{A}_{ln,kj}^{(2*)}$ are given in the Appendix. In

comparison with the case of homogeneous solvent, the matrices $\mathbf{A}^{(1*)}(t)$ and $\mathbf{A}^{(2*)}(t)$ appear in place

of the usual propagation matrices $\mathbf{A}^{(1)}$ and $\mathbf{A}^{(2)}$ [24]. In fact, it can be shown that the sum over the

tensor elements equals those previous propagation matrices, i.e., $\sum_l \mathbf{A}_{l,kj}^{(1*)} = \mathbf{A}_{kj}^{(1)}$ and

$\sum_{l,n} \mathbf{A}_{1n,kj}^{(2*)} = \mathbf{A}_{kj}^{(2)}$. This can be expected because the constant homogeneous solvent conditions

should emerge as a special case from Eq. 8 when constant buoyancy and relative viscosity

coefficients are used. Eq. 8 can be solved with methods similar to those described earlier for the

case of a moving frame of reference [24] and for the Claverie scheme [25]. For time-dependent

density and viscosity gradients, the propagation matrices have to be updated after each time-

increment. The finite element solution was incorporated in the software SEDFIT, which can be

downloaded from www.analyticalultracentrifugation.com.

Dynamic density gradients formed by sedimenting co-solutes

Gradients in density and viscosity can be established during the centrifugation experiment by

sedimentation of a co-solute in high concentration. The mutual diffusion coefficient of such a

component is given by

$$D = \frac{kTv}{f} \left(1 + w \frac{d \ln \gamma}{dw} \right) \qquad (9)$$

where k is the Boltzmann constant, T is the absolute temperature, v is the dissociation number, f

the frictional coefficient, γ the thermodynamic activity coefficient, and w the weight concentration

of the co-solute [38]. Following the approximation that the frictional coefficient for sedimentation and diffusion is approximately identical for the solutes under consideration, such as CsCl, the sedimentation coefficient can be written as

$$s = \frac{M(1-\bar{v}\rho_0)D}{vRT\left(1+wd\ln\gamma/dw\right)} \qquad (10)$$

(with M denoting the molar mass of the species and ρ_0 the solvent density)[20]. Minton has given polynomial approximations for the sedimentation and mutual diffusion coefficient of CsCl solutions, and applied them to the simulation of self-forming CsCl density gradients using a finite difference solution of the Lamm equation [20]. A similar approach is implemented in SEDFIT, using the polynomial approximations for the concentration dependence of *D(c)* and *s(c)* combined with a finite element solution of the Lamm equation [25, 39]. For the simulation of sedimentation of a dilute macromolecular component in the self-forming density gradient, the evolution of the co-solute is coupled to the solution of the Lamm equation for the macromolecular components, and from the local concentration of the co-solute the local density and viscosity experienced by the macromolecular component is calculated.

As an alternative approach, SEDFIT allows one to empirically model experimental data from the redistribution of a co-solute, assign a molar loading concentration of this species, and use its redistribution as a basis for calculating $\rho(r,t)$ and $\eta(r,t)$. This approach is simpler, as it does not require the measurement of the full concentration dependence *D(c)* and *s(c)*. Apparent *D* and *s*-values at the loading concentration may be modeled, for example, to interference optical data of the co-solute alone with water as an optical reference, run separately in the same rotor. Although this approach may appear less rigorous, it is sufficient to calculate the local density and viscosity effects if the co-solute redistribution can be described well.

Results

Because the Lamm equation is notoriously difficult to solve and no analytical solution exists, it is crucial to verify the precision and the limitations of the algorithm. The present method was tested according several different criteria. First, the sedimentation of a 200 kDa protein in a linear density and viscosity gradient was simulated, sufficient to generate a band with neutral buoyancy at ~ 7.1 cm. Both the static and the moving frame of reference algorithms independently converged to the same solution. While static frame of reference algorithm converged rapidly with finer spatial grid (maximal relative error $\delta_{max} < 10^{-5}$ at grid size n > 500), the moving frame of reference required a significantly finer spatial grid to converge to the same solution ($\delta_{max} < 3 \times 10^{-4}$ at n = 20000, $\delta_{max} = 5 \times 10^{-3}$ at n = 1000). This indicates that the moving frame of reference does not lend itself to sedimentation under conditions that include regions of neutral buoyancy. However, this effect was significantly reduced in shallower density gradients that do not lead to band formation. Under these conditions, the moving frame of reference was advantageous when solving the Lamm equation for large macromolecules that sediment rapidly. As a second test of the algorithm, it was verified that mass conservation is fulfilled, and that it solved the Lamm equation correctly for the special cases of constant viscosity and density, which is identical to the sedimentation homogeneous solvent after correction of s and D to standard conditions. Third, the sedimentation of a macromolecule in a large linear density gradient was simulated, and it was verified that the calculated distribution after long times converged to the thermodynamically predicted equilibrium distribution of a Gaussian band with the correct molar mass and density (Eq. 5.260 of [40]). Finally, the Lamm equation solution was found to be consistent with an approximate analytical solution for the special case of diffusion-free sedimentation in a density gradient from compressible solvents [33].

The model for inhomogeneous media was incorporated in several sedimentation models of SEDFIT for the prediction and modeling of macromolecular sedimentation through a dynamically formed density and viscosity gradient. Two different experimental configurations were explored. Figure 1 (top panel) shows the changes in density across the solution column from the sedimentation of 2.5 M CsCl after conventional uniform loading. As the co-solute concentration increases close to the bottom, conditions for neutral buoyancy and flotation for a protein are generated (top panel, bold line). The calculated sedimentation profiles of a hypothetical 500 kDa protein is shown in the middle and lower panel. The initial sedimentation resembles the ordinary formation of a boundary in the meniscus region and the accumulation of material with a steep gradient close the bottom of the cell. After a short time, however, the increasing density of the co-solute at the bottom causes the macromolecule to float back from the bottom of the cell towards the evolving point of neutral buoyancy. Combined with the continuing sedimentation from the sedimentation boundary in the meniscus region, this process concentrates the protein in a peak that approaches the Gaussian shape well-known for isopycnic sedimentation (Figure 1, middle panel). Clearly, the calculated macromolecular sedimentation profiles contain information about its molar mass, sedimentation coefficient, as well as partial-specific volume.

Even if the co-solute concentration is far below the threshold required to establish neutral buoyancy of the macromolecule, its redistribution can cause significant effects on the macromolecular concentration profiles. This is illustrated in Figure 2, which shows the concentration distribution of a 200 kDa protein sedimenting in 1 M CsCl. While the macromolecular sedimentation takes place, the co-solute also redistributes and spans concentrations from 0.76 M near the meniscus to 1.29 M near the bottom (at the end of the time interval shown in Figure 2). This leads to a deceleration of the sedimentation boundary as

compared to the sedimentation in a uniform solvent (dotted line in Figure 2). More striking is a concentration increase in the 'plateau' region towards the bottom of the cell. This is not due to back-diffusion, but due to the differentially decreasing sedimentation rate with higher radii, a consequence of which is the continuous accumulation of material in the region that forms the plateau in homogeneous solvents. A similar effect has been observed by Dishon et al. in the approximate Lamm equation solutions in the rectangular geometry [17]. However, a qualitatively new feature is a negative slope in the 'plateau' region close to the boundary. This is a result of the dilution of the co-solute, which locally increases the buoyant molar mass and sedimentation coefficient of the macromolecules. This increase can produce sedimentation coefficients higher than those at the hinge point of the co-solute, and thus lead to an accumulation of material at the leading edge of the boundary. This effect was found to be more pronounced with a lower ratio of the macromolecular to the co-solute sedimentation coefficient (Figure 2, lower panel).

The model was implemented in SEDFIT for the non-linear regression of macromolecular sedimentation parameters, given sets of concentration distributions. When normally distributed noise of (1% of the loading signal) was added to the data in Figure 1 and 2, they could be analyzed with the independent species model similar to ordinary sedimentation velocity data in homogeneous solvents, but with the effective partial-specific volume as an additional (optional) fitting parameter (data not shown). All parameters converged to the values underlying the simulations, although slightly slower than in the case of uniform solvents. This is attributed to some correlation between the effective partial-specific volume and the remaining parameters, in particular at the smaller density gradients.

As an experimental test for the validity of the presented model for the sedimentation in dynamic density gradients, sedimentation velocity experiments in cesium chloride solutions were

performed. Figure 3 shows the absorbance profiles of at 83 kDa protein in 1.43 M cesium chloride (initial density 1.183 g/ml). The sedimentation profiles are substantially different from those obtained in dilute solution (data not shown). Qualitatively, the data confirm the predicted deceleration of the boundary and the compression of the scans in the bottom region, as well as the increasing slope of the 'plateau' near the bottom region in the later scans (Figure 3). It should be noted that at the conditions used, this region is free of back-diffusion (as measured by control experiments at lower CsCl concentration). Also visible is the predicted boundary anomaly from the local density decrease in the half of the solution column closer to the meniscus, which leads to a transient small negative slope of the 'plateau' (Figure 3, lower panel). This effect is here less pronounced than calculated in the simulation of Figure 2 due to the larger diffusion coefficient of the protein. However, it has been reproducibly observed in further experiments at high CsCl concentration (data not shown).

For the quantitative analysis, the polynomial expressions of [20] for *D(c)* and *s(c)* were used to predict the sedimentation of CsCl, and the resulting density and viscosity profiles were inserted in the Lamm equation model. Because of the high rotor speed, corrections for the compressibility of water were also included [33] (although this effect is smaller than that of the redistribution of the co-solute). The non-linear regression showed some correlation between the apparent partial-specific volume, the sedimentation coefficient, and the bottom position of the centrifuge cell. Therefore, the $s_{20,w}$ value was held constant at 5.05 S, the value predicted from hydrodynamic modeling of the crystal structure [41], which compares well with the value of 5.01 S measured in phosphate buffered saline (PBS), and the bottom location was estimated from a initial scan of the transmitted intensity. Also fixed were the molar mass and the partial-specific volume of the protein under standard conditions, both calculated from the amino acid sequence.

With the meniscus position and the apparent partial-specific volume ϕ' of the protein in 1.43 M cesium chloride as the only floating parameter, a reasonable fit with a root-mean-square (rms) deviation of 0.0099 OD was achieved (Figure 3, solid lines), with $\phi' = 0.762$ ml/g. (When time-invariant noise was considered in the model, the fit converged to a value of $\phi' = 0.760$ ml/g, with an rms deviation of 0.0064 OD, data not shown). The increase in the apparent partial-specific volume in the presence of 1.43 M cesium chloride would correspond to a hydration of 0.20 g/g, if there was no preferential binding of the co-solute to the protein, although the latter cannot be excluded. Overall, a reasonable quantitative and a very good qualitative agreement of the experimental data with the Lamm equation model was found, supporting the validity of the model.

A second configuration theoretically explored was a self-forming density gradient in the synthetic boundary configuration of analytical zone centrifugation [10]. Figure 4 shows the simulated co-solute and macromolecular distributions for a dilute solution of protein which is layered on top of a solution containing 2.5 M CsCl. Although a relatively small density difference (e.g., from 150 mM NaCl) is sufficient for gravitational stability of the protein layer, the purpose of the high CsCl concentration in the present context is to generate a density gradient that permits isopycnic separation of species with different density [13]. The Top Panel in Figure 4 shows the redistribution of the CsCl, its diffusion into the protein lamella with a steep concentration gradient, and the formation of a concentration gradient along the whole solution column. In this configuration, the CsCl gradient is established more rapidly then in the homogeneous loading conditions (Figure 1). The protein distributions are indicated in the middle and lower panel of Figure 4. Interestingly, due to the steep initial density gradient an initial concentration of the protein in the region of the lamella takes place, analogous to the boundary anomaly in the conventional loading situation. Under some conditions, this effect was predicted to produce a

series of initial band profiles increasing in height, qualitatively consistent with experimental scans (J. Lebowitz, unpublished observation). After this period of concentration, the band broadens again and approaches the position of neutral buoyancy. In the simulations, it was found that the extent of this sharpening effect strongly depends on the initial density gradient, and the macromolecular diffusion and sedimentation coefficient. Small diffusion coefficients were also found to generate stronger asymmetry of the bands. As in the conventional loading configuration, the implementation in SEDFIT permits analytical zone centrifugation data to be modeled to extract molar mass, effective partial-specific volume, and the sedimentation coefficient $s_{20,w}$ from experimental data.

Discussion

The sedimentation of macromolecules through inhomogeneous solvents is of great practical importance, but its theoretical description is highly complex. In the present paper, a new theoretical model is presented for the sedimentation in dynamic gradients from sedimenting co-solutes. For the first time, the model permits the prediction of the complete evolution of the macromolecular concentration profiles across the solution column, and can be used to analyze experimentally measured macromolecular concentration distributions, similar to whole boundary modeling approaches in homogeneous solvents. Although the model is based on several simplifying assumptions, it still captures essential features and provides a realistic picture of the sedimentation process, as judged by the agreement with the experimental data from the sedimentation of a protein in high CsCl solutions.

One limitation of the model is that it is based on the two-component Lamm equation, which is strictly valid only if cross-terms in the diffusion coefficients are negligible (Eq. 1.61-1.63 in [34]). In theory, this requirement is fulfilled in the absence of interaction of the macromolecule with the co-solute, and negligible preferential solvation. Clearly, many conditions where density gradients are used in practice will violate this requirement, and this may constitute a serious drawback for a quantitative analysis of the detailed boundary shapes. However, the analysis of experimental data (Figure 3) indicates that even in the presence of significant preferential solvation, its consequences can apparently be captured well by a change in the macromolecular density increment, or apparent partial-specific volume, without considering flows from cross-diffusion. This indicates that under the conditions used, contributions to the macromolecular flows from cross-diffusion may be small, possibly due to the fact that the relative concentration gradients of the co-solute remain small, even though they can already generate a significant

mechanical effect on the macromolecular buoyancy. Further, the model also neglects the dependence of the solvation on the local co-solute concentration, and treats it instead as being constant throughout the entire sedimentation process. Again, this is approximation may be justified if the relative changes of co-solute concentration remain small throughout the solution column. These simplifications seemed to still provide a realistic picture of the sedimentation process in Figure 3, but more experience will be required to generalize this observation, and to explore if the observed change in buoyancy allows to quantitatively measure hydration or preferential solvation parameters [36]. (It should be noted that these considerations about co-solute sedimentation and redistribution are only of second order or negligible, if the effects of co-solutes are evaluated from a series of experiments with different loading concentrations of co-solute or macromolecules. Also, it should be noted that many co-solutes may not generate significant density gradients.)

Frequently, the characterization of proteins is desired in the presence of high concentrations of co-solutes, where preferential solvation occurs. For example, they may be required for stabilizing proteins, or for density matching of detergents in the study of membrane proteins. Preferential solvation can also be very important in the context of protein-protein interactions induced by protein-solvent interactions [42, 43]. The current method could extend sedimentation velocity as a quantitative tool to conditions where such co-solutes generate density gradients. It should be noted that the whole boundary modeling is exquisitely sensitive and the effect of density gradients may be measured at co-solute concentrations where preferential solvation is absent or small, such as with dynamic density gradients produced by H_2O/D_2O mixtures.

Most of the qualitative features in the macromolecular sedimentation profiles caused by

density gradients are well-known. Beyond flotation and the formation of an isopycnic band,

which usually requires relatively high densities, there are also profound changes in the

sedimentation profiles at much lower densities. These consist in a deceleration of the

sedimentation boundary, which results in the continuous accumulation of macromolecules in the

region where in homogeneous solvents a constant plateau would be formed [17]. This is also

observed in static density gradients from compressible solvents [44, 45]. A boundary anomaly

that is characteristic for the dynamic nature of the density gradient is the local inversion of the

leading edge of the boundary (lower panels in Figure 2 and Figure 3). The inversion is

gravitationally stabilized by the underlying density gradient of the co-solute. This feature may

appear not unlike the Johnston-Ogston effect [46, 47], although the interaction is mediated through

hydrostatic density effects between a sedimenting small co-solute and a macromolecule, rather

than the hydrodynamic interaction between two macromolecules. In analytical zone

centrifugation, the anomaly corresponding to the boundary inversion is an initial sharpening of the

bands to concentrations above the loading concentration.

It is clear that the analysis procedures for uniform solvents cannot be applied to density

gradient sedimentation. Even at co-solute concentrations that do not lead to flotation, the

boundary distortions do not permit modeling without consideration of the gradient. For example,

because of the absence of a true plateau, no weight-average sedimentation coefficients can be

defined through second-moment mass balance consideration [44]. As a first step to enable a more

quantitative interpretation of density gradient centrifugation by direct boundary modeling, the

Lamm equation model was implemented for non-linear regression with the independent species

model of SEDFIT. This requires the prediction of the density gradient, which may be

accomplished by taking sedimentation parameters from tabulated data in the literature, as in the

present work, or by independently measuring the co-solute sedimentation profiles with the interference optical detection system. As can be expected, if sufficiently large gradients exist, this permits the determination of molar mass, sedimentation coefficient, and an effective partial-specific volume. Although the extension of the independent species analysis to a continuous sedimentation coefficient distribution c(s) and molar mass distribution c(M) [30] is possible, this approach was not explored. Since the sedimentation profile in density gradients can depend much stronger on the molar mass and partial-specific volume of the macromolecules than in homogeneous solvents, the approximation of a single weight-average frictional ratio for the entire macromolecular population may not be sufficient to model polydisperse mixtures. At conditions of strong density gradients and macromolecules that are heterogeneous with regard to their density, extensions to multi-dimensional distributions $c(s, \overline{v})$ or $c(s, M, \overline{v})$ may be required. One could expect that sedimentation data from the complete transport process towards an isopycnic separation condition contain enough information to define such an extended characterization of a macromolecular mixture.

Appendix

In the theory section, it was shown that the finite element solutions for sedimentation with

buoyancy and viscosity gradients requires the calculation of tensors

$$\mathbf{A}_{l,kj}^{(1*)} = \int_m^b P_l (\partial P_j/\partial r)(\partial P_k/\partial r) r\, dr \text{ and } \mathbf{A}_{ln,kj}^{(2*)} = \int_m^b P_l P_n P_j (\partial P_k/\partial r) r^2 dr.$$ The functions P are

defined as triangular hat functions according to Eqs. 4, based on a division of the solution column

between the meniscus m and the bottom b into n radial grid points r_k (which can be static and

equidistant, as in the Claverie scheme [37], or logarithmically spaced and time-dependent, as in

the moving frame of reference [24]). Because they are overlapping only for identical or

neighboring elements, the integral $\mathbf{A}_{l,kj}^{(1*)}$ is nonzero only if both l and j equals k, k-1, or k+1.

Similarly, $\mathbf{A}_{ln,kj}^{(2*)}$ is nonzero only if n, l, and j equal k, k-1, or k+1. This considerably simplifies the

calculations. The viscosity gradients $\alpha(t)$ and the buoyancy gradients $\beta(t)$ are expressed through

the vectors $\alpha_l(t)$ and $\beta_n(t)$, respectively, which are defined via Eq. 5 on the same grid of radial

points. This allows analytical expressions to be derived for the matrices $\mathbf{A}^{(1*)}(t) = \sum_l \alpha_l \mathbf{A}_{l,kj}^{(1*)}$

and $\mathbf{A}^{(2*)}(t) = \sum_{l,n} \alpha_l \beta_n \mathbf{A}_{ln,kj}^{(2*)}$: For the corner elements of $\mathbf{A}^{(1*)}(t)$ we obtain

$$\mathbf{A}_{11}^{(1*)} = \frac{r_1(2\alpha_1 + \alpha_2) + r_2(\alpha_1 + 2\alpha_2)}{6(r_2 - r_1)}$$

$$\mathbf{A}_{NN}^{(1*)} = \frac{r_N(2\alpha_N + \alpha_{N-1}) + r_{N-1}(\alpha_N + 2\alpha_{N-1})}{6(r_N - r_{N-1})}$$

(A1a)

and for all other elements

$$\mathbf{A}_{k,k-1}^{(1*)} = \frac{r_k(2\alpha_k + \alpha_{k-1}) + r_{k-1}(\alpha_k + 2\alpha_{k-1})}{6(r_{k-1} - r_k)}$$

$$\mathbf{A}_{k,k+1}^{(1*)} = \frac{r_k(2\alpha_k + \alpha_{k+1}) + r_{k+1}(\alpha_k + 2\alpha_{k+1})}{6(r_k - r_{k+1})}$$

(A1b)

$$\mathbf{A}_{k,k}^{(1*)} = -\mathbf{A}_{k,k-1}^{(1)} - \mathbf{A}_{k,k+1}^{(1)}$$

For the corner elements of $\mathbf{A}^{(2*)}(t)$, we obtain

$$\mathbf{A}_{1,1}^{(2*)} = -\frac{\beta_1 \alpha_1}{60}(10r_1^2 + 4r_2 r_1 + r_2^2) - \frac{\beta_2 \alpha_1 + \beta_1 \alpha_2}{60}(2r_1^2 + 2r_2 r_1 + r_2^2)$$
$$- \frac{\beta_2 \alpha_2}{60}(r_1^2 + 2r_2 r_1 + 2r_2^2)$$

$$\mathbf{A}_{2,1}^{(2*)} = -\mathbf{A}_{1,1}^{(2*)}$$

$$\mathbf{A}_{N,N}^{(2*)} = \frac{\beta_{N-1} \alpha_{N-1}}{60}(r_N^2 + 2r_N r_{N-1} + 2r_{N-1}^2) + \frac{\beta_N \alpha_N}{60}(r_N^2 + 4r_N r_{N-1} + 10r_N^2)$$
$$+ \frac{\beta_N \alpha_{N-1} + \beta_{N-1} \alpha_N}{60}(2r_N^2 + 2r_N r_{N-1} + r_{N-1}^2)$$

$$\mathbf{A}_{N-1,N}^{(2*)} = -\mathbf{A}_{N,N}^{(2*)}$$

(A2a)

and for all other elements

$$\mathbf{A}_{k,k-1}^{(2*)} = \frac{\beta_{k-1} \alpha_{k-1}}{60}(r_k^2 + 4r_k r_{k-1} + 10r_{k-1}^2) + \frac{\beta_k \alpha_{k-1} + \beta_{k-1} \alpha_k}{60}(r_k^2 + 2r_k r_{k-1} + 2r_{k-1}^2)$$
$$+ \frac{\beta_k \alpha_k}{60}(2r_k^2 + 2r_k r_{k-1} + r_{k-1}^2)$$

$$\mathbf{A}_{k,k+1}^{(2*)} = -\frac{\beta_k \alpha_k}{60}(2r_k^2 + 2r_k r_{k+1} + r_{k+1}^2) - \frac{\beta_k \alpha_{k-1} + \beta_{k-1} \alpha_k}{60}(r_k^2 + 2r_k r_{k+1} + 2r_{k+1}^2)$$
$$- \frac{\beta_{k+1} \alpha_{k+1}}{60}(r_k^2 + 4r_k r_{k+1} + 10r_{k+1}^2)$$

(A2b)

$$\mathbf{A}_{k,k}^{(2*)} = \frac{\beta_{k-1} \alpha_{k-1}}{60}(r_k^2 + 2r_k r_{k-1} + 2r_{k-1}^2) + \frac{\beta_k \alpha_{k-1} + \beta_{k-1} \alpha_k}{60}(2r_k^2 + 2r_k r_{k-1} + r_{k-1}^2)$$
$$+ \frac{\beta_k \alpha_k}{60}(10r_k^2 + 4r_k r_{k-1} + r_{k-1}^2) - \frac{\beta_k \alpha_k}{60}(10r_k^2 + 4r_k r_{k+1} + r_{k+1}^2)$$
$$- \frac{\beta_k \alpha_{k-1} + \beta_{k-1} \alpha_k}{60}(2r_k^2 + 2r_k r_{k+1} + r_{k+1}^2) - \frac{\beta_{k+1} \alpha_{k+1}}{60}(r_k^2 + 2r_k r_{k+1} + 2r_{k+1}^2)$$

If buoyancy and viscosity gradients are absent and all α_l and β_n equal unity, these elements

$\mathbf{A}^{(1*)}(t)$ and $\mathbf{A}^{(2*)}(t)$ are identical to the matrices $\mathbf{A}^{(1)}$ and $\mathbf{A}^{(2)}$ for homogeneous solvent as given

in Eqs. A2 and A3 in [24] and [49].

Interestingly, the tensor $\mathbf{A}_{1,kj}^{(1*)} = \int_m^b P_l(\partial P_j / \partial r)(\partial P_k / \partial r) r dr$ underlying the matrix $\mathbf{A}^{(1*)}(t)$

is identical to the tensor $\mathbf{W}_{kj,l}$ that was previously used to describe diffusion fluxes of

macromolecules with hydrodynamic or thermodynamic non-idealities (Eq. A6 in [24]); essentially

it describes any radially dependent diffusion. No relationship of the tensor $\mathbf{A}_{\mathrm{ln,kj}}^{(2*)}$ with any tensor

previously used in the context of sedimentation is known. As an alternative to the approach

presented here, it should be possible to also express the sedimentation fluxes in the presence of

density and viscosity gradients within the framework previously derived for concentration

dependent sedimentation (i.e. using the tensors $\mathbf{U}_{\mathrm{kji}}$ defined in Eq. A5 in [24]), if one reduces the

product of the local viscosity and buoyancy into a single radial-dependent factor. However, as can

be seen from the cross-terms of neighboring buoyancy and viscosity coefficients in Eq. A2b

above, this approach would exhibit lower accuracy. Further, use of the previously described

framework with tensors $\mathbf{U}$ and $\mathbf{W}$ is numerically less efficient, in particular for static solvent

gradients. It is more advantageous, therefore to employ the expressions for the matrices $\mathbf{A}^{(1*)}$ and

$\mathbf{A}^{(2*)}$ given above to replace the ordinary propagation matrices $\mathbf{A}^{(1)}$ and $\mathbf{A}^{(2)}$ as described in the

theory section.

These matrix elements, their relationships, and the corresponding expressions in C code

were derived using the symbolic mathematics toolbox of MATLAB (The Mathworks, Natick,

MA), and can be obtained from the author on request.

References

[1]   M. Meselson and F. W. Stahl, The replication of DNA in Escherichia coli, Proc. Natl. Acad. Sci. U S A 44 (1958) 671

[2]   C. Schildkraut, J. Marmur and P. Doty, Determination of the base composition of deoxyribonucleic acid from its buoyant density in CsCl, J. Mol. Biol. 4 (1962) 430-443

[3]   J. Vinograd, J. Lebowitz, R. Radloff, R. Watson and P. Laipis, The twisted circular form of polyoma viral DNA, Proc. Nat. Acad. Sci. 53 (1965) 1104-1111.

[4]   J. B. Ifft, Sedimentation equilibrium of proteins in density gradients, Biophys Chem 5 (1976) 137-157

[5]   O. Clay, N. Carels, C. Douady, G. Macaya and G. Bernardi, Compositional heterogeneity within and among isochores in mammalian genomes. I. CsCl and sequence analyses, Gene 276 (2001) 15-24

[6]   O. Clay, Standard deviations and correlations of GC levels in DNA sequences., Gene 276 (2001) 33-38

[7]   G. Bucciarelli and G. Bernardi, An ultracentrifugation analysis of two hundred fish genomes, Gene 295 (2002) 153-62

[8]   A. Lustig, A. Engel and M. Zulauf, Density determination by analytical ultracentrifugation in a rapid dynamic gradient - application to lipid and detergent aggregates containing proteins, Biochem. Biophys. Acta 1115 (1991) 89-95

[9]   Z. Bozoky, L. Fulop and L. Kohidai, A short-run new analytical ultracentrifugal micromethod for determining low-density lipoprotein sub-fractions using Schlieren refractometry, Eur Biophys J 29 (2001) 621-7

[10] J. Lebowitz, M. Teale and P. Schuck, Analytical band centrifugation of proteins and
      protein complexes, Biochem. Soc. Transact. 26 (1998) 745-749

[11] J. Lebowitz, M. S. Lewis and P. Schuck, Modern analytical ultracentrifugation in protein
      science: a tutorial review, Protein Sci 11 (2002) 2067-79

[12] W. Mächtle (1992) *in* Analytical Ultracentrifugation in Biochemistry and Polymer
      Science. (S. E. Harding, A. J. Rowe and J. C. Horton, Eds.), pp. 147-175, The Royal
      Society of Chemistry, Cambridge.

[13] R. Bruner and J. Vinograd, The evaluation of standard sedimentation coefficients of
      sodium RNA and sodium DNA from sedimentation velocity data in concentrated NaCl and
      CsCl solutions, Biochim.Biophys.Acta 108 (1965) 18-29

[14] C. R. McEwen, Tables for estimating sedimentation through linear concentration gradients
      of sucrose solution, Anal. Biochem. 20 (1967) 114-149

[15] R. W. Clark, Calculation of s20,w values using ultracentrifuge sedimentation data from
      linear sucrose gradients, an improved, simplified method, Biochem. Biophys. Acta 428
      (1976) 269-274

[16] W. Hirst and R. A. Cox, The construction and analysis of sucrose gradients for use with
      zonal rotors, Biochem. J. 159 (1976) 259-265

[17] M. Dishon, G. H. Weiss and D. A. Yphantis, Kinetics of sedimentation in a density
      gradient, Biopolymers 10 (1971) 2095-2111

[18] O. Lamm, Die Differentialgleichung der Ultrazentrifugierung, Ark. Mat. Astr. Fys. 21B(2)
      (1929) 1-4

[19] W. K. Sartory, H. B. Halsall and J. P. Breillatt, Simulation of gradient and band
      propagation in the centrifuge, Biophys. Chem. 5 (1976) 107-135

[20]   A. P. Minton, Simulation of the time course of macromolecular separations in an ultracentrifuge. I. Formation of a cesium chloride denisty gradient at 25°C, Biophys. Chem. 42 (1992) 13-21

[21]   J. S. Philo, An improved function for fitting sedimentation velocity data for low molecular weight solutes, Biophys. J. 72 (1997) 435-444

[22]   J. Behlke and O. Ristau, Molecular mass determination by sedimentation velocity experiments and direct fitting of the concentration profiles, Biophys. J. 72 (1997) 428-434

[23]   W. F. Stafford, Time difference sedimentation velocity analysis of rapidly reversible interacting systems: Determination of equilibrium constants by global non-linear curve fitting procedures, Biophys. J. 74(2) (1998) A301

[24]   P. Schuck, Sedimentation analysis of noninteracting and self-associating solutes using numerical solutions to the Lamm equation, Biophys. J. 75 (1998) 1503-1512

[25]   P. Schuck, C. E. MacPhee and G. J. Howlett, Determination of sedimentation coefficients for small peptides, Biophys. J. 74 (1998) 466-474

[26]   P. Schuck and D. B. Millar, Rapid determination of molar mass in modified Archibald experiments using direct fitting of the Lamm equation, Anal. Biochem. 259 (1998) 48-53

[27]   P. Schuck and B. Demeler, Direct sedimentation analysis of interference optical data in analytical ultracentrifugation., Biophys. J. 76 (1999) 2288-2296

[28]   B. Demeler, J. Behlke and O. Ristau, Determination of molecular parameters from sedimentation velocity experiments: Whole boundary fitting using approximate and numerical solutions of the Lamm equation, Methods in Enzymology 321 (2000) 36-66

[29]   P. Schuck and P. Rossmanith, Determination of the sedimentation coefficient distribution by least-squares boundary modeling, Biopolymers 54 (2000) 328-341

[30]   P. Schuck, Size distribution analysis of macromolecules by sedimentation velocity ultracentrifugation and Lamm equation modeling, Biophys. J. 78 (2000) 1606-1619

[31]   P. Schuck, M. A. Perugini, N. R. Gonzales, G. J. Howlett and D. Schubert, Size-distribution analysis of proteins by analytical ultracentrifugation: strategies and application to model systems, Biophys J 82 (2002) 1096-1111

[32]   J. Behlke and O. Ristau, A new approximate whole boundary solution of the Lamm differential equation for the analysis of sedimentation velocity experiments, Biophys Chem 95 (2002) 59-68

[33]   P. Schuck, submitted (this is the accompanying paper)

[34]   H. Fujita (1962) Mathematical Theory of Sedimentation Analysis, Academic Press, New York.

[35]   E. F. Cassassa and H. Eisenberg, Thermodynamic analysis of multicomponent systems, Adv. Protein Chem. 19 (1964) 287-395

[36]   C. Ebel, H. Eisenberg and R. Ghirlando, Probing protein-sugar interactions, Biophys J 78 (2000) 385-93

[37]   J.-M. Claverie, H. Dreux and R. Cohen, Sedimentation of generalized systems of interacting particles. I. Solution of systems of complete Lamm equations, Biopolymers 14 (1975) 1685-1700

[38]   C. Tanford (1961) Physical chemistry of macromolecules., Wiley, New York.

[39]   J.-M. Claverie, Sedimentation of generalized systems of interacting particles. III. Concentration-dependent sedimentation and extension to other transport methods, Biopolymers 15 (1976) 843-857

[40]   H. Fujita (1975) Foundations of ultracentrifugal analysis, John Wiley & Sons, New York.

[41]   J. Garcia De La Torre, M. L. Huertas and B. Carrasco, Calculation of hydrodynamic

        properties of globular proteins from their atomic-level structure, Biophys J 78 (2000) 719-

        30

[42]   L. Costenaro and C. Ebel, Thermodynamic relationships between protein-solvent and

        protein-protein interactions, Acta Crystallogr D Biol Crystallogr 58 (2002) 1554-9

[43]   L. Costenaro, G. Zaccai and C. Ebel, Link between protein-solvent and weak protein-

        protein interactions gives insight into halophilic adaptation, Biochemistry 41 (2002)

        13245-52

[44]   H. K. Schachman (1959) Ultracentrifugation in Biochemistry, Academic Press, New York.

[45]   H. Fujita, J. Am. Chem. Soc. 63 (1956) 1092

[46]   J. P. Johnston and A. G. Ogston, A boundary anomaly found in the ultracentrifugal

        sedimentation of mixtures, Trans. Faraday Soc. 42 (1946) 789-799

[47]   J. J. Correia, M. L. Johnson, G. H. Weiss and D. A. Yphantis, Numerical study of the

        Johnston-Ogston effect in two-component systems, Biophys Chem 5 (1976) 255-264

[48]   J. Vinograd and J. E. Hearst, Equilibrium sedimentation of macromolecules and viruses in

        a density gradient, Fortschritte der Chemie organischer Naturstoffe 20 (1962) 372-422

[49]   D. J. Cox and R. S. Dale (1981) *in* Protein-protein interactions. (C. Frieden and L. W.

        Nichol, Eds.), Wiley, New York.

[50]   M. J. Rosovitz, P. Schuck, M. Varughese, A. P. Chopra, Y. Singh, L. M. McGinnis and S.

        H. Leppla, Alanine Scanning Mutations in Anthrax Toxin Protective Antigen Domain 4

        Reveal Residues Important for Binding to the Cellular Receptor and to a Neutralizing

        Monoclonal Antibody, (submitted)

[51]   R. C. Weast (1972) Handbook of Chemistry and Physics., CRC Press, Cleveland, OH.

Figure Legends

Figure 1: Sedimentation in a self-forming density gradient in conventional loading configuration.

Top Panel: Calculated density profiles generated by the sedimentation of 2.5 M CsCl at 60,000

rpm (in time-intervals of 600 sec). The initial density is 1.31 g/ml, which is below the density of

neutral buoyancy for a protein of partial-specific volume 0.73 ml/g. With time, the increase in

concentration close to the bottom generates densities that permit flotation of the protein. The

evolution of the point of critical density (1.37 g/ml) is shown as a bold solid line, and its

projection to the radius-time plane as a dotted line. Middle Panel: Sedimentation profiles of a

protein with a molar mass of 500 kDa, a partial-specific volume of 0.73 ml/g, and a sedimentation

coefficient of $s_{20,w}$ = 18 S. Shown are the concentration distributions at 300 sec (solid line), 3,000

sec (dashed line), 6,000 sec (dotted line), 9,000 sec (dash-dotted line), 12,000 sec (solid line),

15,000 sec (dashed line), and 30,000 sec (dotted line). Lower Panel: Contour plot of the

evolution of the macromolecular concentration distribution. (It should be noted that the time-scale

is in 10^4 sec, which does not permit resolving the very early stages that are included in the middle

panel.) The bold dotted line indicates the radii with neutral buoyancy conditions calculated from

the sedimentation of the co-solute, as shown in the Top Panel.

Figure 2: Sedimentation in a self-forming density gradient in conventional loading configuration

with lower concentration of co-solute. Top Panel: Concentration distributions calculated for a

200 kDa protein ($\bar{v}$ = 0.73 ml/g, $s_{20,w}$ = 10 S) sedimenting at 60,000 rpm in 1 M CsCl. Data are

shown with time-intervals of 600 sec. For comparison, the sedimentation profiles calculated for a

constant homogeneous solvent at ρ = 1.126 g/ml and η = 0.952 mPa×s (the density and viscosity

of 1 M CsCl) are shown as dotted lines. Lower Panel: Detailed view of the plateau region of the

calculated concentration profiles for a protein of 150 kDa with a sedimentation coefficient $s_{20,w}$ of

5 S sedimenting at 60,000 rpm in 1 M CsCl.

Figure 3: Experimental absorbance profiles from the sedimentation of a protein in a dynamic

density gradient (circles) and best-fit model (solid lines). Anthrax protective antigen [50] was

diluted at a concentration of 0.45 mg/ml into PBS with 1.43 M CsCl (initial density 1.183 g/ml),

and sedimented at a rotor speed of 60,000 rpm and a rotor temperature of 25 °C in an Optima

XLA/I analytical ultracentrifuge (Beckman Coulter, Fullerton, CA). Data shown in the upper

panel are the absorbance profiles measured at 280 nm in time intervals of 730 sec. The data were

modeled using finite element Lamm equation solutions for the sedimentation of CsCl (with the

polynomial approximations for the non-ideal sedimentation parameters reported in [20]), together

with tabulated data for the concentration dependences of the density and viscosity of CsCl

solutions [51] for dynamically updating the local density and viscosity in the Lamm equation

solution Eq. 8 for the sedimentation of the protein. Also included were corrections for the

compressibility of water [33]. For fitting the data, the known protein molar mass and the partial

specific volume $\bar{v}$ from the amino acid sequence was used, and its sedimentation coefficient $s_{20,w}$

was fixed to the value of 5.05 S predicted from the crystal structure [41]. The apparent partial

specific volume ϕ' was treated as fitting parameters (together with the meniscus of the solution

column), converging to a value of 0.762 ml/g with a final root mean square deviation of the fit of

0.0099 OD. The lower panel provides a more detailed view of the boundary anomaly due to the

hydrostatic interaction of the protein and the co-solute: the experimental scans at 2570 sec (solid

line) and 4030 sec (circles) are shown and the corresponding theoretical profiles (for clarity, the

scans are offset).

Figure 4: Simulated analytical zone centrifugation in a self-forming density gradient. The distributions are calculated for a 1 mm layer of a protein solution in PBS on top of a 9 mm solution of PBS with 2.5 M CsCl, at 60,000 rpm and 25 °C. For the protein, a molar mass of 82.7 kDa, a $s_{20,w}$ –value of 5 S, and $\bar{v}$ = 0.77 ml/g was assumed, with a loading concentration of 1. Top Panel: Calculated redistribution of CsCl with time. Middle Panel: Protein distributions at time intervals of 3000 sec (first distribution shown at 300 sec). The dotted line indicates the protein layer at the start of centrifugation. Lower Panel: Contour plot of the evolution of the protein concentration distribution.
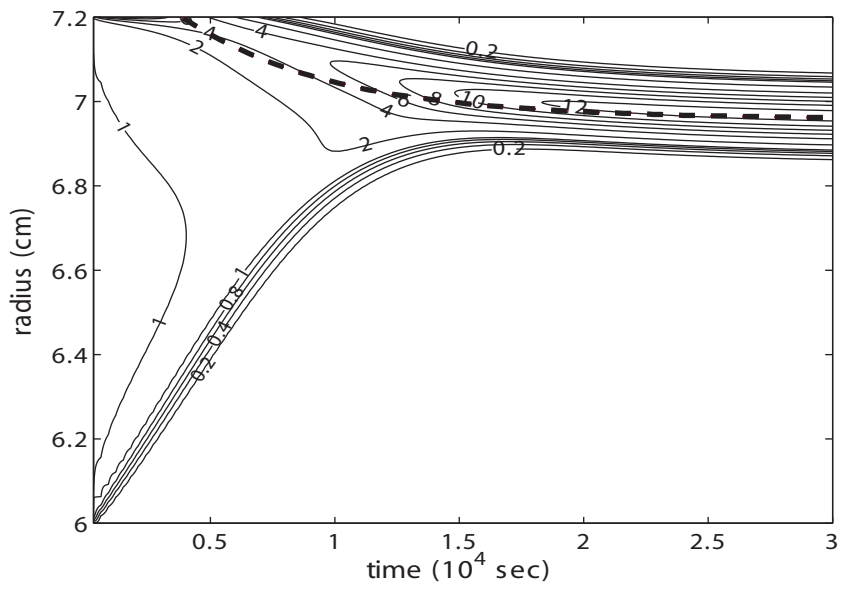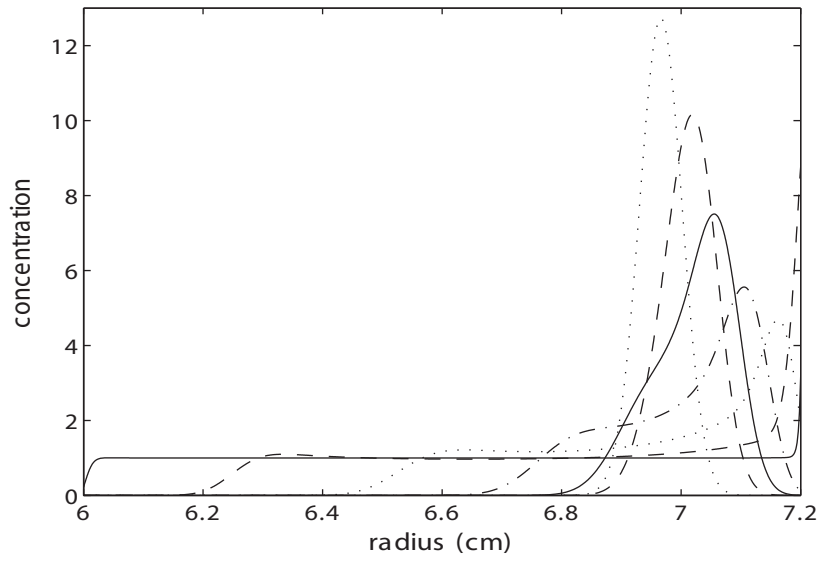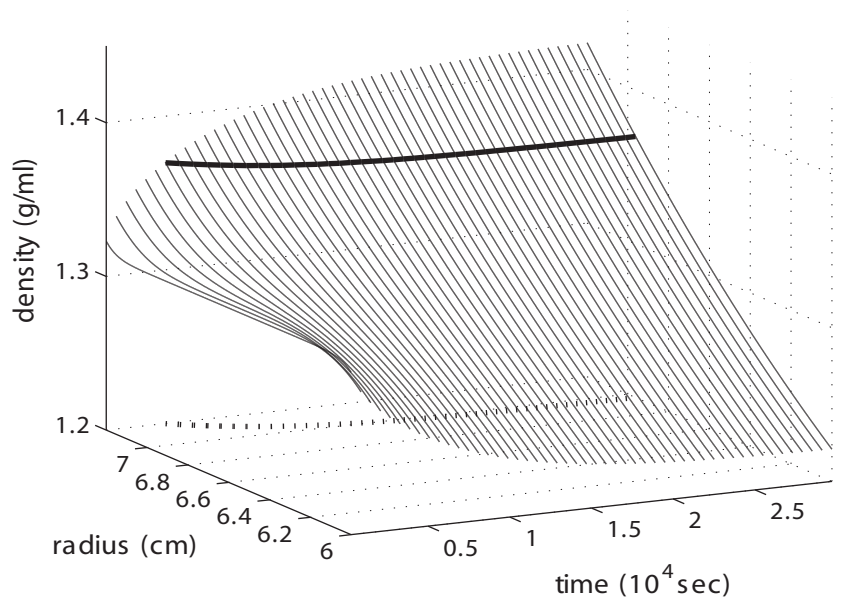
Figure 1
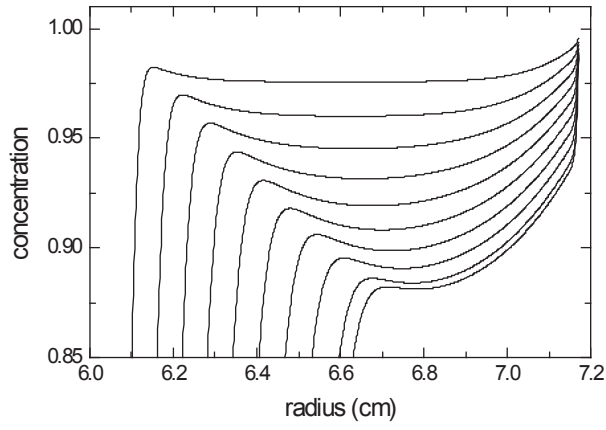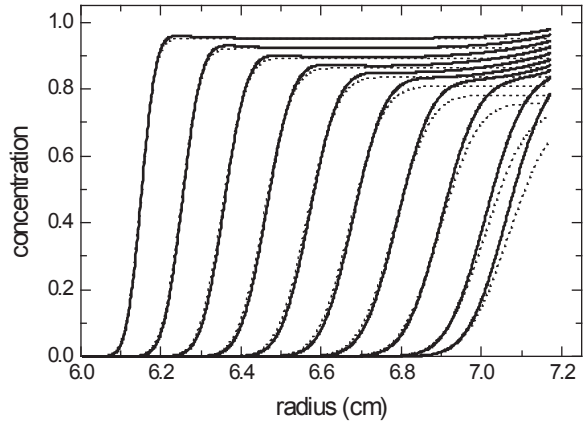
Figure 2

Figure 3

Figure 4